Molecular Therapy
Nucleic Acids
Original Article

Reducible PEG-POD/DNA Nanoparticles for Gene Transfer In Vitro and In Vivo: Application in a Mouse Model of Age-Related Macular Degeneration

Bhanu Chandar Dasari,[1] Siobhan M. Cashman,[1] and Rajendra Kumar-Singh[1]

[1]Department of Developmental, Molecular, and Chemical Biology, Program in Genetics, Sackler School of Graduate Biomedical Sciences, Tufts University School of Medicine, 136 Harrison Avenue, Boston, MA 02111, USA

Non-viral gene delivery systems are being developed to address limitations of viral gene delivery. Many of these non-viral systems are modeled on the properties of viruses including cell surface binding, endocytosis, endosomal escape, and nuclear targeting. Most non-viral gene transfer systems exhibit little correlation between in vitro and in vivo efficiency, hampering a systematic approach to their development. Previously, we have described a 3.5 kDa peptide (peptide for ocular delivery [POD]) that targets cell surface sialic acid. When functionalized with polyethylene glycol (PEG) via a sulfhydryl group on the N-terminal cysteine of POD, PEG-POD could compact plasmid DNA, forming 120- to 180-nm homogeneous nanoparticles. PEG-POD enabled modest gene transfer and rescue of retinal degeneration in vivo. Systematic investigation of different stages of gene transfer by PEG-POD nanoparticles was hampered by their inability to deliver genes in vitro. Herein, we describe functionalization of POD with PEG using a reducible orthopyridyl disulfide bond. These reducible nanoparticles enabled gene transfer in vitro while retaining their in vivo gene transfer properties. These reducible PEG-POD nanoparticles were utilized to deliver human FLT1 to the retina in vivo, achieving a 50% reduction in choroidal neovascularization in a murine model of age-related macular degeneration.

INTRODUCTION

During the previous decade, there has been significant progress in the field of gene therapy.[1–5] Much of this has been fueled by the successful application of adeno-associated virus (AAV) as a gene transfer vector.[6] Despite this progress, critical challenges to the application of AAV in gene therapy persist, namely a significantly limited transgene capacity,[7] immunotoxicity,[8] and hepatotoxicity,[9] as well as the cost of production and standardization of these novel biologics.[10] To address the limitations of AAV and other viral vectors, a surge of interest in the development of non-viral gene transfer technologies has led to the identification of an expansive repertoire of polymers, peptides, and lipids with gene transfer capability.[11] However, while these formulations lead to efficient gene transfer to cells in vitro, they have not generally been found to deliver transgenes efficiently in vivo, particularly to post-mitotic cells such as neurons in the brain or the retina.[12,13]

Similar to viral vectors, non-viral gene transfer vectors need to efficiently package DNA, dock at the cell surface, become endocytosed, escape the endosome, and enter the nucleus to enable transgene expression.[14] A single non-viral agent that efficiently replicates all of these steps has thus far not been identified, and it is likely that a successful non-viral vector will require multiple components to overcome different aspects of the delivery process, from cell targeting to nuclear entry.[15] Non-viral DNA delivery vectors will, therefore, need to be systematically assembled rather than identified. The process of non-viral vector development has been hampered by the lack of correlation of in vitro transfection data with that observed in vivo,[12,13] and in-depth analysis of the interaction of non-viral vectors with each step of the delivery pathway, from cell surface to nucleus, is technically challenging in vivo.[16] Bridging the gap between in vitro and in vivo gene transfer efficiency is, therefore, critical to the development of non-viral gene delivery systems. Previously, we have described a novel peptide known as peptide for ocular delivery (POD) that can efficiently compact DNA and enable gene transfer to cells in culture.[17] These POD/DNA nanoparticles, however, failed to deliver DNA to post-mitotic cells in vivo.[18] We determined that the addition of polyethylene glycol (PEG) to POD prior to complexing with DNA led to the formation of homogeneous nanoparticles of approximately 120–150 nm in size, not substantially larger than an adenovirus (~100 nm).[18] We found that these PEGylated POD/DNA nanoparticles could now enable delivery of DNA to retinal cells of mice and attenuate the progression of light-induced apoptosis and ensuing retinal degeneration in a murine model of retinitis pigmentosa.[18,19] Relative to viral vectors, however, the levels and duration of transgene expression are limited, needing further development before PEG-POD/DNA nanoparticles could be considered to have clinical potential. Continued development of PEG-POD/DNA nanoparticles, however, has been hampered by their inability to transfect cells in vitro.

Received 14 February 2017; accepted 8 June 2017;
http://dx.doi.org/10.1016/j.omtn.2017.06.004.

Correspondence: Rajendra Kumar-Singh, Department of Developmental, Molecular, and Chemical Biology, Program in Genetics, Sackler School of Graduate Biomedical Sciences, Tufts University School of Medicine, 136 Harrison Avenue, Boston, MA 02111, USA.
E-mail: rajendra.kumar-singh@tufts.edu

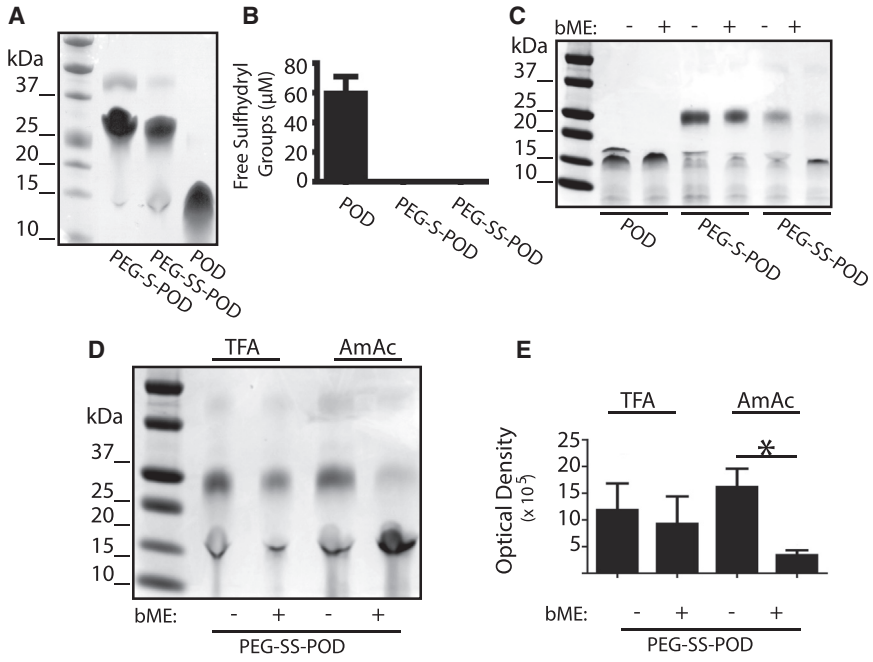

Figure 1. Characterization of PEG-S-POD and PEG-SS-POD

(A) SDS-PAGE analysis of PEG (10 kDa) conjugation with POD using PEG-MALM to generate PEG-S-POD or PEG-OPSS to generate PEG-SS-POD. The 3.5 kDa POD peptide forms a pentamer that migrates at ~17.5 kDa. PEGylated POD, in the form of PEG-S-POD or PEG-SS-POD, is observed to migrate predominantly at ~27.5 kDa. A faint band is observed at ~37.5 kDa for both PEG-S-POD and PEG-SS-POD indicating the addition of two PEG moieties per POD pentamer in both conjugation reactions. (B) Quantitation of reactive sulfhydryl groups using Ellman's reagent (DTNB) following PEG conjugation with POD using thiol-reactive PEG moieties PEG-MALM and PEG-OPSS shows that the free sulfhydryls of POD peptide are efficiently reacted with PEG reagents to generate PEG-S-POD and PEG-SS-POD, respectively. (C) SDS-PAGE analysis of POD, PEG-S-POD, and PEG-SS-POD following incubation in the presence or absence of 5 mM β-mercaptoethanol (β-ME) shows efficient reduction of the disulfide bond of PEG-SS-POD (27.5 kDa) to release POD pentamer (~17.5 kDa). Incubation of PEG-S-POD with β-ME has little or no effect on conjugate, with most of the conjugate migrating as the PEGylated POD pentamer (~27.5 kDa). (D) SDS-PAGE analysis of PEG-SS-POD equilibrated with either trifluoroacetic acid (TFA) or ammonium acetate (AmAc) shows that the disulfide bond is less efficiently reduced by β-ME to release the ~17.5 kDa POD pentamer in the presence of TFA buffer than in the presence of AmAc buffer. (E) Optical density analysis of SDS-PAGE shows that AmAc equilibrated PEG-SS-POD has a significant increase (*$p < 0.05$) in the ratio of the unPEGylated POD pentamer (~17.5 kDa):PEGylated POD (27.5 kDa) relative to that of TFA equilibrated PEG-SS-POD, indicating a more efficient reduction of the disulfide bond by β-ME when in the presence of AmAc buffer. Quantitation was performed on three independent SDS-PAGE analyses. Data are presented as mean ± SE. PEG, polyethylene glycol; POD, peptide for ocular delivery.

In the current study, we describe the development of a *reducible* PEGylated POD/DNA nanoparticle that enables gene transfer in vitro and in vivo. This novel nanoparticle is subject to disruption of the PEG-POD bond by the extracellular environment. The reducible PEG-POD/DNA nanoparticle (PEG-SS-POD/DNA) has the same structure and DNA binding capacity as the previously described non-reducible PEGylated nanoparticle but exhibits efficient gene transfer in vitro without adversely affecting its transfection efficiency of the murine retina in vivo. The reducible PEG-SS-POD/DNA nanoparticles were used to deliver a transgene expressing soluble FLT1, an isoform of vascular endothelial growth factor (VEGF) receptor 1,[20] to cells in culture and to murine retina, and were shown to significantly reduce growth of neovascular lesions in a murine model of choroidal neovascularization (CNV). These reducible PEG-SS-POD/DNA nanoparticles provide a critical step toward understanding the obstacles to intracellular trafficking using in vitro data that can be applied to post-mitotic cells in vivo.

RESULTS

Conjugation of PEG to POD Peptide with a Reducible Disulfide Bond

Previously we attached a 10 kDa PEG to the free sulfhydryl group on the N-terminal cysteine residue of POD using the maleimide group of methoxy-PEG-maleimide (mPEG-MALM).[18] This PEG-POD conjugation, involving a thioether bond, is hereafter referred to as PEG-S-POD. To determine whether conjugation of PEG with POD using a reducible disulfide bond restores transfection of cells by PEG-POD/DNA nanoparticles in vitro, we attached PEG to POD using an orthopyridyl disulfide functionalized 10 kDa PEG (methoxy-PEG-orthopyridyl disulfide [mPEG-OPSS]). This PEG-POD we hereby refer to as PEG-SS-POD. Following purification on a size exclusion column, conjugation of PEG with POD was confirmed by PAGE (Figure 1A). Previously we have shown that the 3.5 kDa POD migrates at a position corresponding to ~17.5 kDa,[18] likely because of formation of a pentamer. Consistent with addition of a 10 kDa PEG to the pentamer, PEG-S-POD migrates at a position on the gel corresponding to ~27.5 kDa (Figure 1A). A band of reduced intensity migrating at ~37.5 kDa is also observed for PEG-S-POD (Figure 1A), likely caused by the attachment of an additional PEG to the POD pentamer.[18] When POD is conjugated with mPEG-OPSS, the majority of the PEG-SS-POD complex also migrates at ~27.5 kDa, with some of the PEG-SS-POD also observed migrating at ~37.5 kDa (Figure 1A).

To compare the efficiency of PEG conjugation with POD using mPEG-OPSS instead of mPEG-MALM, we employed Ellman's reagent/dithionitrobenzoic acid (DTNB) to measure free sulfhydryl groups in each reaction (Figure 1B). Sulfhydryl quantitation revealed no free sulfhydryl groups in either the PEG-S-POD or PEG-SS-POD reactions, indicating that PEG conjugation occurs with comparable efficiencies using mPEG-MALM or mPEG-OPSS (Figure 1B).

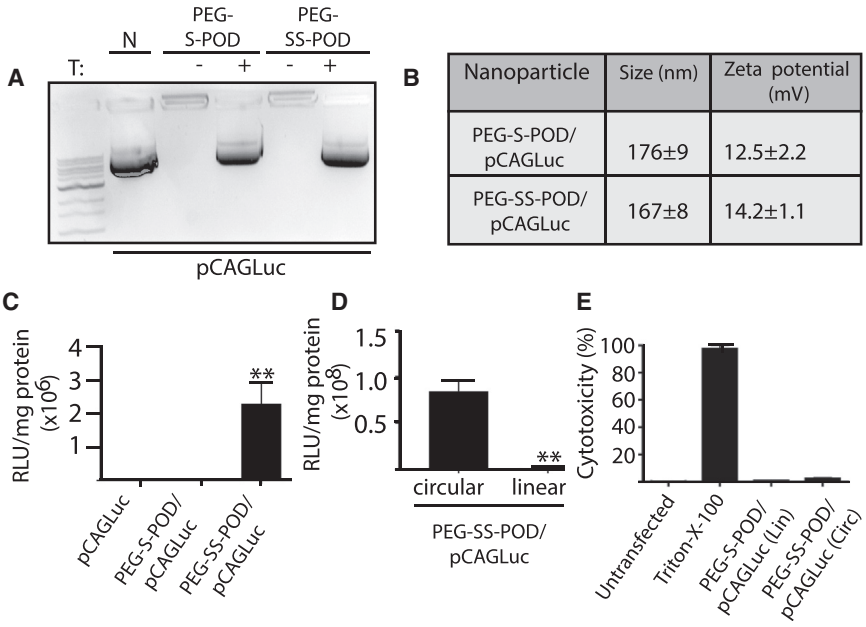

Figure 2. PEG-SS-POD, but Not PEG-S-POD, Particles Efficiently Transfect ARPE-19 Cells In Vitro

(A) Agarose gel retardation analysis shows compaction of luciferase expressing plasmid, pCAGLuc, by PEG-S-POD and PEG-SS-POD. In the absence of trypsin (T), pCAGLuc compacted with either PEG-S-POD or PEG-SS-POD is prevented from migrating in the gel, because of neutralization of negatively charged DNA by positively charged POD peptide. Pre-incubation of the nanoparticles with trypsin (T) to digest the POD releases the pCAGLuc plasmid for migration in the gel. (B) Analysis of nanoparticle size and zeta potential by dynamic light scatter shows that PEG-S-POD/pCAGLuc and PEG-SS-POD/pCAGLuc nanoparticles are similar in size (nm, mean ± SD) and colloidal stability (mV, mean ± SD). (C) Quantitation of luciferase activity in extracts of ARPE-19 cells at 24 hr following incubation with either uncompacted pCAGLuc, PEG-S-POD/pCAGLuc nanoparticles, or PEG-SS-POD/pCAGLuc nanoparticles shows a significant ($p = 0.002$) 2,800-fold increase in luciferase activity in cells treated with PEG-SS-POD/pCAGLuc nanoparticles relative to that of cells treated with PEG-S-POD/pCAGLuc nanoparticles. (D) Quantitation of luciferase activity in extracts of ARPE-19 cells following incubation with PEG-SS-POD/pCAGLuc nanoparticles containing either linearized plasmid or circular plasmid shows an 85-fold ($p = 0.002$) lower transfection efficiency when PEG-SS-POD is used to deliver linear plasmid than when used to deliver circular plasmid. (E) LDH assay of ARPE-19 cells incubated with PEG-SS-POD/pCAGLuc nanoparticles indicates low levels of cytotoxicity when nanoparticles contain either linearized (Lin) or circular (Circ) pCAGLuc plasmid. Data are presented as the percentage of dead cells relative to cells treated with the detergent, Triton X-100, which causes 100% cell lysis. Data are presented as mean ± SE, except where otherwise stated. N, naked (uncompacted) DNA; RLU, relative luciferase unit. $^{**}p \leq 0.01$.

To determine the capacity for reduction of the disulfide bond in the PEG-SS-POD, unconjugated POD, PEG-S-POD, and PEG-SS-POD were incubated with the reducing agent, β-mercaptoethanol, and samples were run on an SDS-polyacrylamide gel (Figure 1C). Of the three samples tested, only PEG-SS-POD exhibited a reduction in the ratio of the 27.5 kDa to 17.5 kDa band, corresponding to the PEG-POD conjugate and unconjugated POD, respectively, in the presence of β-mercaptoethanol (Figure 1C). This confirms that the disulfide bond of PEG-SS-POD can be reduced, releasing the POD peptide.

The shape and size of peptide/DNA nanoparticles have been found to depend on whether the peptide is equilibrated with trifluoroacetic acid (TFA) or with ammonium acetate (AmAc) prior to DNA compaction.[21] We, however, have not observed a difference in nanoparticle structure when PEG-S-POD was equilibrated in either buffer (data not shown). However, TFA has been found to inhibit reduction of disulfide bonds.[22] To determine whether the use of either TFA or AmAc as a counterion for equilibration of PEG-SS-POD could inhibit reduction of the disulfide bond, we incubated PEG-SS-POD equilibrated in each buffer with β-mercaptoethanol (Figure 1D). Indeed, we observed that the disulfide bond of PEG-SS-POD (~27.5 kDa) was more efficiently reduced, releasing unconjugated POD pentamer (~17.5 kDa), when suspended in AmAc buffer than when suspended in TFA (Figure 1D). Quantitation of the intensity of the ~27.5 kDa band corresponding to PEG-SS-POD equilibrated in either TFA or AmAc in the presence or absence of β-mercaptoethanol confirmed the higher efficiency of reduction of the disulfide bond in AmAc ($p < 0.05$; Figure 1E).

PEG-SS-POD Does Not Alter the Efficiency or Size of Compacted DNA Nanoparticles

Plasmid DNA encoding luciferase, pCAGLuc, was compacted using PEG-SS-POD in a nitrogen:phosphate (N:P) ratio of 8:1. Plasmid DNA compaction by PEG-SS-POD was confirmed by an inability of the compacted plasmid to migrate in an agarose gel (Figure 2A), because of neutralization of negatively charged DNA by positively charged POD peptide. Incubation of the PEG-SS-POD compacted pCAGLuc plasmid in trypsin prior to gel analysis released the plasmid DNA (Figure 2A). Analysis of the PEG-SS-POD/pCAGLuc nanoparticles by dynamic light scatter (DLS; Figure 2B) indicated that there was no significant difference in the size of these nanoparticles (167 ± 8 nm) relative to the size of PEG-S-POD/pCAGLuc nanoparticles (176 ± 9 nm). Analysis of the zeta potential of the nanoparticles, a measure of their colloidal stability in solution, showed no significant difference between the PEG-S-POD/pCAGLuc (12.5 ± 2.2 mV) and PEG-SS-POD/pCAGLuc (14.2 ± 1.1 mV) nanoparticles; in addition, these values (±10–20 mV) are considered relatively stable.[23] Together, these data indicate the stability of the disulfide bond in PEG-SS-POD following DNA compaction, concentration, and dialysis prior to agarose gel and DLS analysis.

PEG-SS-POD Nanoparticles Mediate Greater In Vitro Gene Transfer Than PEG-S-POD Particles

To determine whether use of the disulfide bond for conjugation of PEG to POD allowed for more efficient cellular uptake and expression of plasmid DNA than conjugation of PEG with POD using a thioether bond, we incubated ARPE-19 cells in 200 ng of uncompacted pCAGLuc, 200 ng of plasmid in PEG-SS-POD/pCAGLuc nanoparticles, or 200 ng of plasmid in PEG-S-POD/pCAGLuc nanoparticles. Twenty-four hours following incubation, the ARPE-19 cells were harvested for quantification of luciferase activity (Figure 2C). As was previously observed,[18] PEG-S-POD/pCAGLuc-incubated cells exhibited no significant difference in luciferase activity relative to those cells incubated with uncompacted pCAGLuc (Figure 2C). However, cells incubated with PEG-SS-POD/pCAGLuc exhibited an ~2,800-fold increase in luciferase activity relative to PEG-S-POD/pCAGLuc-treated cells ($p = 0.002$; Figure 2C).

Plasmid DNA can exist as one of three different topological forms: supercoiled, relaxed circular, and linear.[24] It has been found that these different forms transfect mammalian cells with different levels of efficiency.[25,26] In order to determine whether transfection by POD-SS-PEG/pCAGLuc nanoparticles is influenced by DNA topology, both non-linearized (circular) and linearized pCAGLuc plasmid was compacted using PEG-SS-POD, and the resulting nanoparticles were used to transfect ARPE-19 cells. At 24 hr following transfection, cells were harvested for quantification of luciferase activity (Figure 2D). Luciferase activity in cells incubated in PEG-SS-POD/pCAGLuc (linear plasmid) was observed to be 85-fold ($p = 0.002$) lower relative to cells incubated in PEG-SS-POD/pCAGLuc (circular plasmid) (Figure 2D).

The efficiency with which a reagent transfects cells is generally directly correlated with the amount of cellular toxicity elicited.[27] To determine whether this is also the case for PEG-SS-POD/pCAGLuc nanoparticles, we collected media from ARPE-19 cells transfected with either PEG-SS-POD/pCAGLuc (circular plasmid) nanoparticles or PEG-SS-POD/pCAGLuc (linear plasmid) nanoparticles at 24 hr following incubation in nanoparticles and measured for activity of lactate dehydrogenase (LDH). The amount of toxicity of nanoparticle-treated cells is presented (Figure 2E) as a percentage relative to that of cells treated with the detergent, Triton X-100, in which the LDH activity was considered to represent 100% toxicity. The percentage toxicity observed in both PEG-SS-POD/pCAGLuc (linear plasmid) nanoparticle-incubated cells and cells incubated with PEG-SS-POD/pCAGLuc (circular plasmid) nanoparticles was not observed to be significantly above that of untransfected cells not exposed to nanoparticles (Figure 2E), indicating that the increased transfection efficiency of circular DNA by PEG-SS-POD is not a result of increased toxicity.

Increased Transfection by PEG-SS-POD/DNA Nanoparticles Is the Result of Increased Uptake by Cells In Vitro

Although PEG prevents large aggregate formation in nanoparticle formulations,[28] it is speculated that it can reduce the efficiency with which the attached moiety (in this case, POD) binds its receptor on the cell surface.[29] It has previously been found that the cell culture media provides a reducing environment for disruption of disulfide bonds.[30] To determine whether this could allow for improved transfection efficiency by PEG-SS-POD/pCAGLuc nanoparticles in ARPE-19 cells relative to PEG-S-POD/pCAGLuc nanoparticles because of increased uptake of the PEG-SS-POD/pCAGLuc nanoparticles by the cell, pCAGLuc was labeled with a fluorophore (Cy5) and compacted using either PEG-SS-POD or PEG-S-POD. The resulting nanoparticles were tested for compaction and DNA concentration (data not shown), and added to ARPE-19 cells using equivalent amounts of labeled pCAGLuc. Cells exposed to either PEG-SS-POD/pCAGLuc^{Cy5} nanoparticles or PEG-S-POD/pCAGLuc^{Cy5} nanoparticles were incubated with trypsin at two different time points postexposure, and the cells were resuspended for analysis of Cy5 fluorescence by flow cytometry (Figure 3). At 2 hr (data not shown) and 24 hr (Figure 3) postexposure, cells incubated with uncompacted Cy5-labeled luciferase plasmid indicated very few Cy5-positive cells (1.38%). Of those cells incubated with Cy5-labeled luciferase plasmid delivered using Lipofectamine, 34.5% were positive for Cy5 fluorescence (Figure 3). At 2 hr and 24 hr postexposure, cells treated with PEG-S-POD/pCAGLuc^{Cy5} nanoparticles had 0.08% and 2.1% of cells, respectively, positive for Cy5 signal (Figure 3). Among the cells incubated with PEG-SS-POD/pCAGLuc^{Cy5} nanoparticles, however, 23.8% of cells exhibited Cy5 fluorescence at 2 hr postexposure (Figure 3). At 24 hr postexposure, the number of ARPE-19 cells treated with PEG-SS-POD/pCAGLuc^{Cy5} nanoparticles that indicated Cy5 fluorescence was observed to be 67.4% of the cell population (Figure 3). These data are consistent with the luciferase expression data presented above (Figure 2C) and consistent with the hypothesis that PEG-SS-POD/pCAGLuc nanoparticles are more efficient than PEG-S-POD/pCAGLuc nanoparticles at binding the cell surface for uptake.

The Disulfide Bond in PEG-SS-POD Nanoparticles Is Reduced in the Extracellular Environment

The increased transfection efficiency of PEG-SS-POD/pCAGLuc^{Cy5} nanoparticles in vitro relative to that of PEG-S-POD/pCAGLuc^{Cy5} nanoparticles is consistent with reduction of the disulfide bond in the extracellular environment, release of the PEG moiety, and increased accessibility of the POD for attachment to the cell surface. In order to determine whether extracellular release of PEG occurs, we quantified the amount of both POD and PEG remaining in the cell medium at 4 hr following incubation of ARPE-19 cells with either PEG-SS-POD/pCAGLuc nanoparticles or PEG-S-POD/pCAGLuc nanoparticles. The medium collected after 4 hr of incubation of cells with nanoparticles was analyzed by SDS-PAGE (Figure 4). To detect POD peptide, we stained the gel with Coomassie blue (Figure 4A). A positive control was included on the gel, consisting of the PEG-SS-POD/pCAGLuc nanoparticles that had been pre-incubated with the reactive sulfhydryl donor, cysteine (Figure 4A). As anticipated, PEG-SS-POD/pCAGLuc nanoparticles pre-incubated with cysteine exhibited a band migrating at ~17.5 kDa, consistent with dePEGylated POD peptide. Neither of the unconjugated PEG reagents, mPEG-OPSS nor mPEG-MALM, stained positive with Coomassie

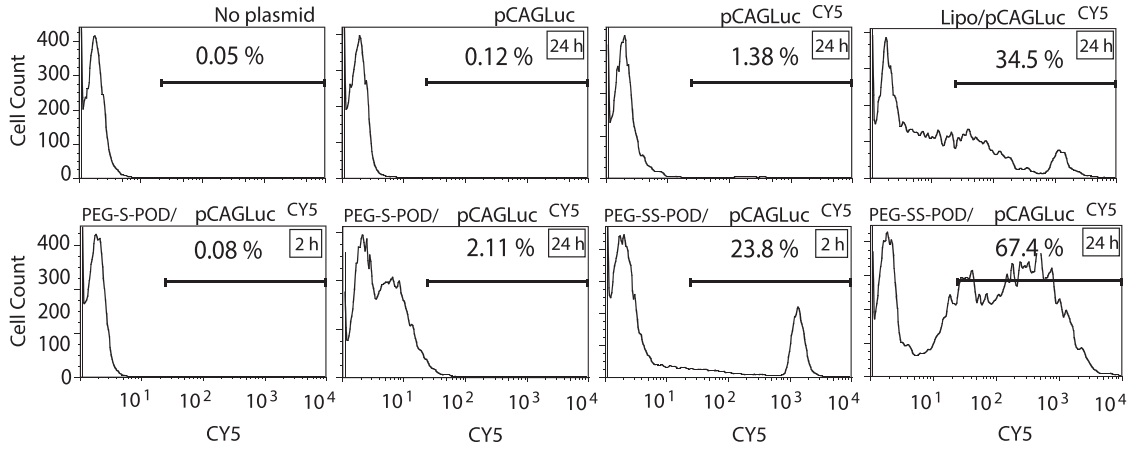

Figure 3. Improved Transfection by PEG-SS-POD/pCAGLuc Nanoparticles Is the Result of More Efficient Uptake

Flow cytometry analysis of the uptake of Cy5-labeled pCAGLuc by ARPE-19 cells incubated with either uncompacted plasmid or plasmid compacted with either PEG-S-POD or PEG-SS-POD. Negative controls included untransfected cells and cells incubated with unlabeled pCAGLuc. Lipofectamine delivery of Cy5-labeled pCAGLuc was used as a positive control. Cells were trypsinized and harvested for analysis at 2 hr and 24 hr postincubation. At 2 hr and 24 hr following incubation with PEG-S-POD/pCAGLuc nanoparticles there was no or low percentage, respectively, of cells with Cy5 fluorescence. Cells treated with PEG-SS-POD/pCAGLuc nanoparticles, however, had ~24% and ~67% of cells positive for Cy5 fluorescence.

blue, and there was no band detected in media from control (untransfected) cells (Figure 4A). The media harvested from cells incubated with PEG-S-POD/pCAGLuc nanoparticles for 4 hr exhibited a band migrating at ~27.5 kDa, consistent with a PEGylated POD complex (Figure 4A). However, in the media harvested from cells incubated with PEG-SS-POD/pCAGLuc nanoparticles for 4 hr, there was no band observed consistent with either PEGylated (27.5 kDa) or dePEGylated (17.5 kDa) POD. These data indicate efficient release of PEG from PEG-SS-POD/pCAGLuc nanoparticles in the extracellular environment and efficient uptake of the dePEGylated POD nanoparticles (Figure 4A).

In order to detect PEG, we performed a second SDS-PAGE and stained with 0.1 N iodine (Figure 4B). As above, unconjugated PEG reagents, mPEG-MALM and mPEG-OPSS, were used as controls; both reagents migrated between 15 and 20 kDa, with the slight difference in migration patterns likely because of the OPSS and MALM side chains. PEG-SS-POD/pCAGLuc nanoparticles pre-incubated with cysteine were also analyzed on the iodine-stained gel; in this lane, a band was observed at ~17 kDa, similar in size to that observed for mPEG-OPSS (Figure 4B). Media collected after 4 hr from cells incubated with PEG-S-POD/pCAGLuc nanoparticles exhibited two bands on the gel: one band migrating at ~17 kDa, consistent with free PEG, and a second band at ~25 kDa, consistent with PEGylated POD (Figure 4B). That some of the PEG conjugated via a thioether bond is released from the PEG-S-POD/pCAGLuc nanoparticles is not unexpected; despite the greater in vivo stability of the thioether linkage relative to that of the disulfide linkage, inefficient reduction of maleimide-thiol conjugates in the physiological environment has been observed.[31] Media collected after 4 hr from cells incubated with PEG-SS-POD/pCAGLuc nanoparticles, however, exhibited only one band, migrating at ~17 kDa, consistent with free PEG. A band consistent with PEGylated POD was not detected in media incubated with PEG-SS-POD/pCAGLuc nanoparticles, indicating efficient reduction of the disulfide bond in the extracellular environment and release of PEG from the PEG-SS-POD/pCAGLuc nanoparticles (Figure 4B). As expected, no bands were detected in media collected from control (untransfected) cells.

In order to determine whether inhibition of thiols in the extracellular environment would adversely affect the efficiency of transfection of cells by PEG-SS-POD/pCAG-Luc nanoparticles, we added cell-impermeable DTNB to the media of ARPE-19 cells and incubated them for 30 min prior to addition of PEG-SS-POD/pCAGLuc nanoparticles. At 24 hr posttreatment with nanoparticles, the ARPE-19 cells were harvested for quantification of luciferase activity (Figure 4C). ARPE-19 cells cultured in media exposed to a 1 mM concentration of DTNB prior to treatment with nanoparticles did not reveal any alteration in luciferase activity relative to cells cultured in media that were not exposed to DTNB prior to addition of nanoparticles (Figure 4C). However, ARPE-19 cells cultured in media pre-exposed to 3 mM DTNB had a significant 85% ($p < 0.05$) reduction in luciferase activity following incubation with PEG-SS-POD/pCAGLuc nanoparticles relative to cells grown in media not exposed to DTNB; this strongly indicates an extracellular reduction of the disulfide bond of PEG-SS-POD/pCAGLuc nanoparticles by thiols in the media as a key mechanism of the increased transfection efficiency of ARPE-19 cells by PEG-SS-POD/pCAGLuc nanoparticles.

PEG-SS-POD/DNA Nanoparticles Can Deliver Plasmid DNA to the Murine Retina In Vivo

Previously we have shown delivery of plasmid to retinal pigment epithelium (RPE) cells in vivo by PEG-S-POD/DNA nanoparticles following subretinal injection.[18,32] In order to determine whether

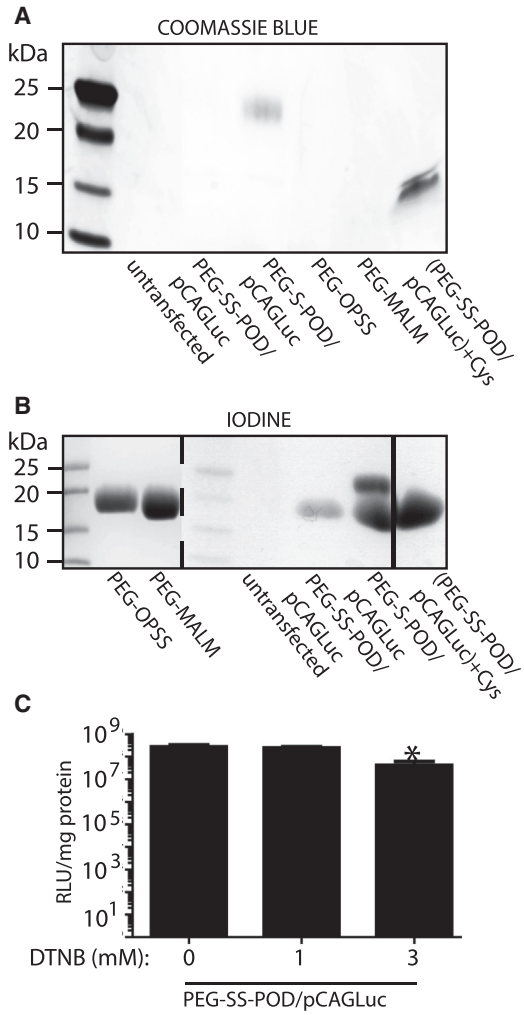

Figure 4. PEG Is Released from PEG-SS-POD in the Extracellular Environment

(A) SDS-PAGE analysis of media harvested from cells 4 hr after incubation with PEG-SS-POD/pCAGLuc or PEG-S-POD/pCAGLuc nanoparticles. Coomassie blue staining of gel detects PEGylated and free POD peptide. Unconjugated PEG does not stain, as evidenced by loading of PEG-MALM and PEG-OPSS. PEG-SS-POD/pCAGLuc nanoparticles pre-incubated with cysteine (Cys) were used as a positive control for POD peptide release from conjugate following reduction of disulfide bond; this band is observed to migrate as expected for POD pentamer. Media from cells treated with PEG-S-POD/pCAGLuc nanoparticles show a band migrating at ~25 kDa indicating the presence of PEGylated POD. Media from cells treated with PEG-SS-POD/pCAGLuc nanoparticles, however, show no detectable band at 25 kDa. The absence of a band consistent with dePEGylated POD indicates that most of the dePEGylated POD/pCAGLuc nanoparticles have been taken up by the cells at 4 hr. (B) SDS-PAGE analysis of the same samples described in (A); this gel, however, was stained with iodine solution for detection of PEG. The free PEG reagents, PEG-OPSS and PEG-MALM, migrate at ~17 kDa. PEG-SS-POD/pCAGLuc nanoparticles pre-incubated with cysteine (Cys) show a similar 17 kDa band, indicating reduction of the disulfide bond and release of PEG from the nanoparticle. Media from cells treated with PEG-S-POD/pCAGLuc nanoparticles show two bands, one migrating at ~17 kDa and the other band migrating at ~25 kDa, indicating the presence of both free PEG and PEG-S-POD. Media from cells treated with PEG-SS-POD/pCAGLuc nanoparticles shows only one band, which migrates at ~17 kDa, consistent with free PEG. The absence of a band migrating at 25 kDa is consistent with the observations of the Coomassie-stained gel above. (C) Quantitation of luciferase activity in extracts of ARPE-19 cells incubated in the presence of 0, 1, and 3 mM cell-impermeable DTNB prior to transfection with PEG-SS-POD/pCAGLuc nanoparticles. A significant 85% reduction (*$p < 0.05$) in transfection efficiency was observed when cells were pre-incubated with 3 mM DTNB prior to addition of nanoparticles. Data are presented as mean ± SE.

the reducible disulfide PEG-SS-POD linkage impacts delivery of plasmid DNA to the murine RPE, pCAGLuc was compacted with either PEG-SS-POD or PEG-S-POD, and the resulting nanoparticles were injected into the subretinal space of BALB/cJ mice. Forty-eight hours postinjection, the posterior eyecups of injected mice were harvested and assayed for luciferase activity (Figure 5A). Relative to eyes injected with uncompacted pCAGLuc, eyes injected with the non-reducible PEG-S-POD/pCAGLuc nanoparticles exhibited a 21-fold increase in luciferase activity (Figure 5A). Eyes injected with the reducible PEG-SS-POD/pCAGLuc nanoparticles exhibited a similar increase (23-fold) in luciferase activity (Figure 5A) relative to eyes injected with uncompacted plasmid. These data indicate that conjugation of PEG to the nanoparticle via a reducible linker does not adversely affect gene transfer in vivo.

Our data also suggest that either reduction of the disulfide bond to release PEG from the PEG-SS-POD/pCAGLuc nanoparticles does not occur as efficiently in the in vivo extracellular environment as in the in vitro environment, or that PEG "shielding" of the nanoparticle is not the major limiting factor to transfection in vivo. Once the initial barrier to cell entry imposed by the plasma membrane is overcome, the nanoparticle is faced with a new challenge in encountering the nuclear membrane. A critical difference between ARPE-19 cells in vitro and RPE cells of the mouse eye is that the ARPE-19 cells are actively dividing with concomitant breakdown of the nuclear membrane, likely allowing access of the plasmid DNA and/or nanoparticle to the nucleus. RPE cells of the adult murine eye are largely mitotically quiescent,[33] providing no such easy access to the nucleus. Injury to the retina, however, has been shown to induce RPE cell proliferation through the process of epithelial-to-mesenchymal transition (EMT);[34] one such injury is laser-induced photocoagulation of murine RPE.[35,36] In order to determine whether transfection of RPE in vivo by PEG-SS-POD/pCAGLuc nanoparticles could be enhanced by induction of RPE cell division by laser-induced photocoagulation, we injected C57BL/6J mice in the subretinal space with PEG-SS-POD/pCAGLuc nanoparticles either without laser treatment or immediately following laser treatment. Two days postinjection, eyecups were harvested and the posterior eyecup assayed for luciferase activity (Figure 5B). Following quantification, eyes injected with PEG-SS-POD/pCAGLuc nanoparticles following laser treatment exhibited a 389% increase ($p = 0.008$) in luciferase activity relative to that of eyes injected with PEG-SS-POD/pCAGLuc nanoparticles without laser treatment.

In an attempt to determine the cell type transfected by PEG-SS-POD/DNA nanoparticles in laser-treated mice, a lacZ-expressing plasmid

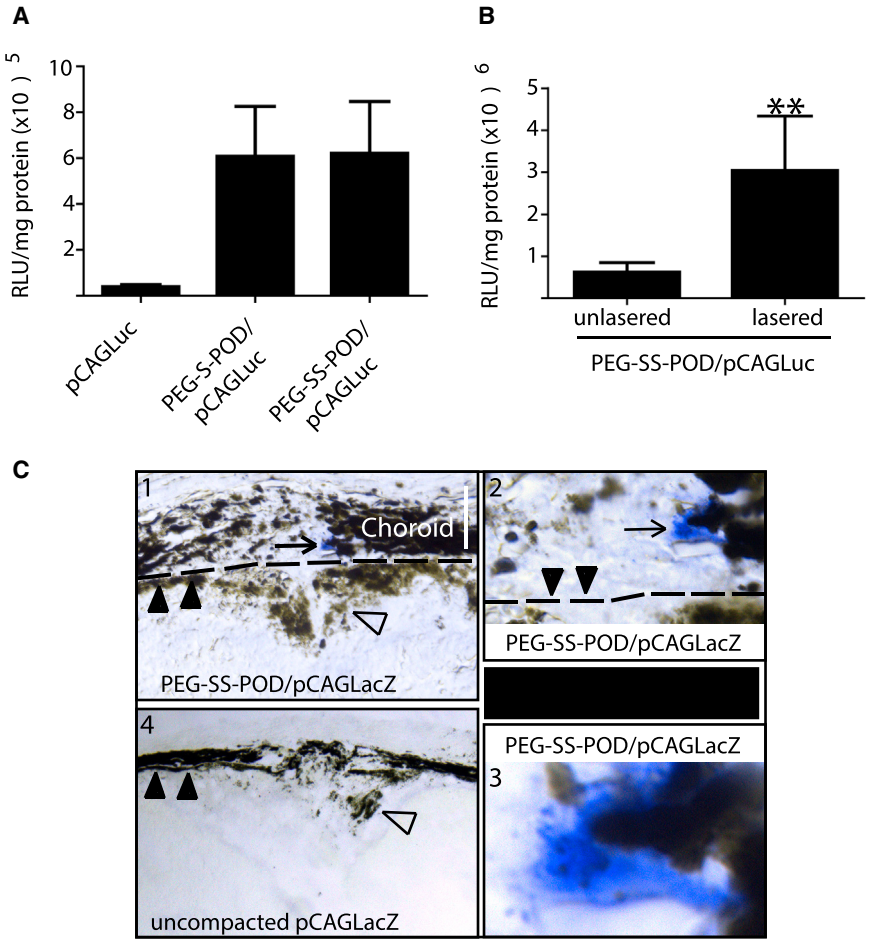

Figure 5. PEG-SS-POD/DNA Nanoparticles Can Transfect the Murine RPE In Vivo

(A) Quantitation of luciferase activity in extracts of RPE/choroid from mice 2 days following subretinal injection with either uncompacted pCAGLuc, PEG-S-POD/pCAGLuc nanoparticles, or PEG-SS-POD/pCAGLuc nanoparticles shows a 21-fold and 23-fold increase, respectively, in transfection efficiency of the nanoparticles relative to uncompacted plasmid. (B) Quantitation of luciferase activity in extracts of RPE/choroid from untreated and laser-treated mice following subretinal injection with PEG-SS-POD/pCAGLuc nanoparticles shows a 389% increase ($p = 0.008$) in luciferase expression in eyecups of laser-treated mice relative to that of untreated mice. $^{**}p \leq 0.01$. (C) Retinal cryosections of eyes injected with either PEG-SS-POD/pCAGLacZ nanoparticles or uncompacted pCAGLacZ plasmid following laser treatment. (C1) Retinal section of PEG-SS-POD/pCAGLacZ-injected eye shows lacZ-positive cell (arrow) in the choroid. Closed arrowheads mark the single RPE cell layer, whereas open arrowheads denote the area of disruption of the RPE cell layer. Dotted line denotes border between RPE and choroid. (C2) Higher magnification of lacZ-positive cell (arrow) shows more clearly that it occurs within the choroid and not below the boundary with the RPE (denoted by the dotted line). (C3) Further magnification confirms the absence of pigment in the lacZ-positive cell, excluding the likelihood of transfection of a choroidal melanocyte. (C4) Retinal section of eye injected with uncompacted pCAGLacZ plasmid shows the absence of lacZ-positive cells in the choroid or in the RPE. Closed arrowheads mark the single RPE cell layer, whereas open arrowheads denote the area of disruption of the RPE cell layer. n = 5 eyes for each treatment. Data are presented as mean ± SE.

(pCAGLacZ) was compacted using PEG-SS-POD and injected into the subretinal space of mice immediately following laser treatment. At 48 hr post-laser treatment, injected eyes were harvested for in situ enzyme assay for lacZ activity in the whole eyecup, followed by cryosectioning (Figure 5C). In PEG-SS-POD/pCAGLacZ-injected eyes, occasional lacZ-positive cells were observed only within the region of laser damage (Figure 5C1, arrow). The scarcity of lacZ-positive cells observed was not consistent with the increase in luciferase activity observed in laser-treated eyes relative to that of untreated eyes following injection of PEG-SS-POD/DNA nanoparticles; it is likely, therefore, that the in situ lacZ activity assay is not sufficiently sensitive to detect all transfected cells. The few lacZ-positive cells detected were observed within the choroid (Figures 5C1 and C2, arrows) and were devoid of pigment (Figures 5C2 and C3, arrow). Eyes injected with uncompacted pCAGLacZ plasmid were not found to have lacZ-positive cells (Figure 5C4).

PEG-SS-POD-Mediated Delivery of Plasmid Expressing Soluble FLT1 Ameliorates Laser-Induced CNV

In addition to causing RPE cell proliferation, laser photocoagulation of the murine RPE induces proliferation of endothelial cells, resulting in CNV through increased expression of VEGF.[37] Laser-induced CNV is the most commonly utilized animal model of the "wet" form of age-related macular degeneration,[38] the most common cause of blindness among people over the age of 65 years. In order to determine whether the transfection efficiency of PEG-SS-POD/DNA nanoparticles following laser photocoagulation is therapeutically relevant, we compacted a plasmid expressing human soluble FLT1 (hFLT1) using PEG-SS-POD and injected it into the subretinal space of C57BL/6J mice immediately following laser treatment, and the effect on growth of CNV was quantified. The plasmid employed, pCAGhFLT1, was generated to express hFLT1 from a chicken β-actin promoter/CMV enhancer. Prior to compaction, expression of hFLT1 from pCAGhFLT1 was confirmed by western blot analysis of media harvested from ARPE-19 cells at 24 hr postinfection with either pCAGhFLT1 or a control plasmid, pCAGLuc (Figure 6A). Media from pCAGhFLT1 transfected cells showed a specific band at ~120 kDa (Figure 6A), consistent with previous analyses of glycosylated soluble FLT1.[20] Media from untransfected cells and cells transfected with pCAGLuc exhibited no detectable bands. Cells transfected with pUNO1-hFLT1(s7) were used as a positive control (Figure 6A) for expression of hFLT1. Compaction of pCAGhFLT1 with

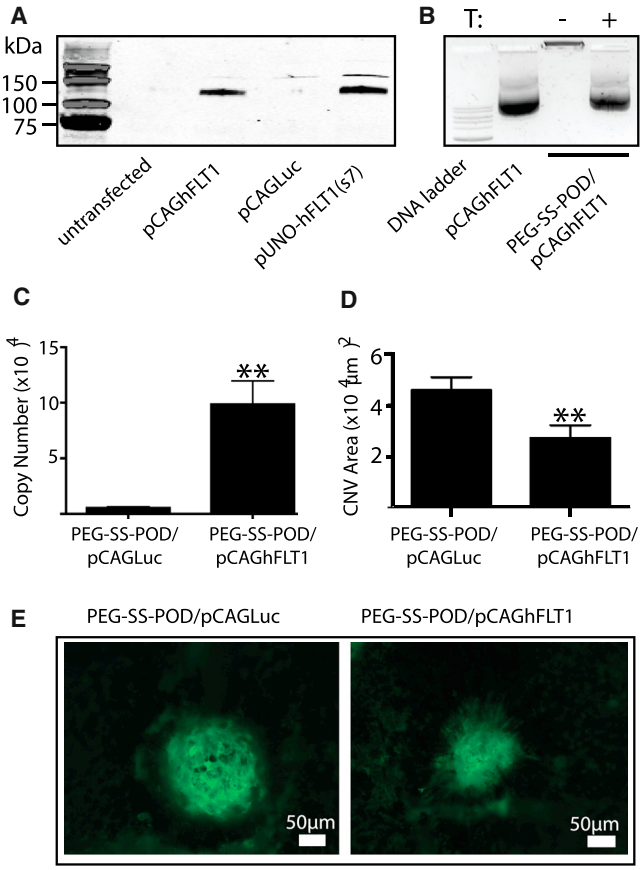

Figure 6. Subretinal Delivery of PEG-SS-POD/pCAGhFLT1 Nanoparticles Reduces CNV

(A) Western blot analysis of hFLT1 in media of untransfected cells or cells transfected with either pCAGhFLT1, pCAGLuc, or pUNO-hFLT1(s7) shows the presence of a unique band migrating at ~120 kDa, consistent with glycosylated hFLT1, in media of cells transfected with hFLT1 encoding plasmids, but not in media of controls. (B) Agarose gel retardation analysis of the compaction of pCAGhFLT1 by PEG-SS-POD. Uncompacted pCAGhFLT1 is loaded as a control. PEG-SS-POD/pCAGhFLT1 nanoparticles show retardation in the gel, consistent with efficient compaction. Pre-incubation of the nanoparticles with trypsin (T) releases the pCAGhFLT1 plasmid for migration in the gel. (C) qRT-PCR of FLT1 expression in murine eyecups at 2 days after laser and injection of PEG-SS-POD/pCAGhFLT1 nanoparticles shows a significant presence of FLT1 mRNA. Copy number of mRNA was determined using a standard curve of predetermined copy number of pCAGhFLT1. (D) Quantitation of the area of CNV in eyecups of mice at 7 days following injection of either PEG-SS-POD/pCAGhFLT1 nanoparticles or control (PEG-SS-POD/pCAGLuc) nanoparticles shows a significant ~50% reduction ($p = 0.007$) in the size of CNV in mice injected with PEG-SS-POD/pCAGhFLT1 nanoparticles relative to CNV size of control injected mice. n = 70 spots for naked plasmid injection; n = 68 spots for PEG-SS-POD~pCAGEN-hFLT1 injections. (E) Representative micrographs of CNV lesions stained with FITC-GSL I from eyecups of mice injected with either PEG-SS-POD/pCAGhFLT1 nanoparticles or PEG-SS-POD/pCAGLuc nanoparticles. Data are presented as mean ± SE. $^{**}p \leq 0.01$.

PEG-SS-POD was confirmed by an agarose gel retardation analysis (Figure 6B). Pre-incubation of the nanoparticles with trypsin prior to gel electrophoresis released the pCAGhFLT1 for migration in the gel (Figure 6B). Following confirmation of the integrity of the plasmid and nanoparticles, C57BL/6J mice were administered laser treatment and immediately injected in the subretinal space with either PEG-SS-POD/pCAGhFLT1 or PEG-SS-POD/pCAGLuc nanoparticles. At 2 days after laser followed by injection of the nanoparticles, the posterior eyecups of some of the mice were harvested for analysis of hFLT1 expression (Figure 6C). qRT-PCR of extracted RNA showed a significant ($p = 0.003$) level of expression of hFLT1 mRNA, as measured by the number of copies of hFLT1 mRNA, in PEG-SS-POD/pCAGhFLT1-injected eyes after laser relative to control injected eyes (Figure 6C). Seven days following injection, eyes of the remaining mice were harvested and the size of CNV growth quantified by staining of RPE/choroid with the endothelial-specific lectin, *Griffonia Simplicifolia* lectin I (GSL I; Figures 6D and 6E). Following quantification of the CNV area, eyes injected with PEG-SS-POD/pCAGhFLT1 nanoparticles exhibited an ~50% reduction in CNV area relative to eyes injected with PEG-SS-POD/pCAGLuc nanoparticles ($p = 0.007$).

DISCUSSION

Previously, we have found that PEGylation of POD/DNA nanoparticles was necessary for delivery of the nanoparticle to RPE cells in vivo.[18] Conjugation of PEG to the nanoparticle, however, abolished its capacity for transfection of cells in vitro.[18] Herein, we discovered that use of a reducible PEG-POD/DNA nanoparticle (PEG-SS-POD), in which PEG is attached to the nanoparticle via a disulfide linker, allowed for a very significant increase in transfection of ARPE-19 cells in vitro relative to a non-reducible PEGylated POD/DNA nanoparticle (PEG-S-POD), without adversely affecting gene transfer efficiency to the murine eye in vivo. This reducible PEG-SS-POD/DNA nanoparticle should provide a valuable tool to study intracellular trafficking of the relevant POD/DNA complex in cells in vitro.

Importantly, our data demonstrate that the increased transfection efficiency of PEG-SS-POD/DNA relative to that of PEG-S-POD/DNA is unlikely due to alterations in nanoparticle structure—i.e., size of the particle or DNA-condensing capacity of the PEG-SS-POD—or to an increase in cellular toxicity of the PEG-SS-POD/DNA nanoparticle. The increased in vitro transfection by the PEG-SS-POD/DNA relative to PEG-S-POD/DNA nanoparticles was found to be coincident with increased cellular uptake of the reducible nanoparticle by ARPE-19 cells. A reduction of ARPE-19 cell transfection by PEG-SS-POD/DNA nanoparticles following inhibition of thiols in the media, as well as the detection of free PEG and not POD-conjugated PEG in the media of PEG-SS-POD/DNA-incubated cells, strongly implicates release of PEG in the extracellular environment in the increased cellular uptake of plasmid DNA in vitro.

These data are consistent with a study investigating the effect of a reducible PEG conjugation on DNA delivery using polylysine, CK30.[30] That study found a 10-fold increase in transfection efficiency of the reducible nanoparticle was very likely due exclusively to the release of PEG by thiols in the extracellular rather than intracellular

environment and subsequent aggregation of nanoparticles on the cell surface.[30] To our knowledge, such nanoparticles have not yet been tested in vivo.

In our study, the reducible linkage in PEG-SS-POD did not impact transfection by PEG-SS-POD/DNA nanoparticles of murine RPE in vivo. While this is possibly due to differences in redox potential between the in vivo and in vitro extracellular environments, it has been found that cells grown in vitro condition the media such that the redox state is similar to that of the extracellular matrix in vivo.[39] It is, therefore, more likely that the difference in performance of the reducible nanoparticles in vitro versus in vivo is due to the mitotic status of the RPE cells. To date, nanoparticles conjugated with PEG via a disulfide linkage have only been delivered to mitotic cells in vivo.[40,41] When liposomes conjugated with the reducible linker were delivered intravenously to a murine model of B cell lymphoma, the "reducible" liposomes had an improved therapeutic efficacy relative to "non-reducible" liposomes,[40] despite a reduced stability in the plasma, likely because of PEG release by blood components such as cysteine. In vivo gene transfer to a murine model of glioblastoma using a reducible PEGylated polymer was also increased following intravenous injection, albeit a "modest" increase, relative to that of the non-reducible PEGylated polymer;[41] the modest increase is likely also due to increased clearance of the reducible polymer in the plasma.

In the case of subretinal injection, however, nanoparticles are delivered adjacent to the RPE and, therefore, stability of nanoparticles in plasma is not a significant concern. That the PEG-S-POD/DNA and PEG-SS-POD/DNA nanoparticles exhibit equivalent competency in gene transfer to the murine eye following subretinal injection suggests that release of PEG is not a critical factor for subretinal delivery to RPE cells. Changing the proliferative status of cells in the choroid and RPE in vivo by laser photocoagulation[35,36] resulted in a significant increase in transfection by PEG-SS-POD/DNA nanoparticles, suggesting that the nuclear membrane is a more significant barrier than the plasma membrane to DNA delivery in vivo. This increase in transfection efficiency by the reducible nanoparticles is therapeutically relevant and was sufficient to reduce the growth of neovascular lesions in the laser-induced CNV, a murine model for the wet form of AMD.

Laser photocoagulation induces its effects through absorption of energy by melanin in the choroidal melanocytes and RPE cells;[36] the melanocytes and RPE cells are damaged by the heat that ensues, inducing a burst of cellular proliferation among surrounding RPE cells, as well as vascular endothelial cells in the choroid and macrophages, and microglia in the retina and choroid.[36] Following subretinal injection of PEG-SS-POD/pCAGLuc nanoparticles in lasered mice, a significant increase in luciferase-positive cells was observed relative to non-lasered mice. It is possible that, similar to other studies investigating reducible nanoparticles in vivo,[40,41] extracellular release of PEG from the PEG-SS-POD/DNA nanoparticles in the laser-damaged choroid increases susceptibility of the dePEGylated particles to uptake by infiltrating macrophages and/or microglia. The absence of pigment in the lacZ-positive cells, as well as their location in the choroid, of lasered mice injected with PEG-SS-POD/DNA nanoparticles is consistent with uptake of the nanoparticles by either macrophages or microglia. The possibility of transfection of endothelial cells by these particles was excluded by the absence of staining of lacZ-positive cells with GSL I (data not shown).

Considering the efficiency with which PEG-SS-POD/DNA nanoparticles reduce the size of CNV lesions in laser-treated mice, however, we consider it likely that the number of cells observed positive for lacZ activity in PEG-SS-POD/pCAGLacZ-injected eyes is an underestimate. Previous studies indicate that subretinal injection of an AAV-8 vector expressing soluble FLT1 prior to laser treatment of mice resulted in an ~38% reduction in the size of CNV lesions.[42] Considering the efficiency of RPE and photoreceptor transduction by AAV-8 shown in the study[42] relative to the efficiency of ocular transfection of PEG-SS-POD/DNA nanoparticles as indicated by lacZ staining, the difference in the percentage of reduction in CNV size in our study (~50%) versus the AAV-8 study is more likely explained by a lack of sensitivity of the detection of lacZ-positive cells in laser-treated eyes pre-injected with PEG-SS-POD/pCAGLacZ nanoparticles.

Laser photocoagulation of C57Bl6/J mice results in a process of CNV mediated by increased levels of VEGF[41] and is a much exploited murine model of neovascular AMD.[38] Soluble FLT1 is a naturally occurring isomer of VEGF receptor 1[43] and has been found to reduce the progression of CNV in the murine and non-human primate models of laser-induced CNV.[42,44] The efficiency with which PEG-SS-POD/DNA nanoparticles expressing a growth-factor-inhibiting protein are observed to inhibit aberrant cellular proliferation in the murine eye suggests that the PEG-POD/DNA nanoparticles may warrant further investigation in proliferative retinopathies, such as proliferative vitreoretinopathy, proliferative diabetic retinopathy, and neovascular AMD.

In summary, we have generated a reducible PEG-SS-POD/DNA nanoparticle that efficiently transfects cells in vitro without negatively impacting transfection of cells in vivo. We have found that the increase in in vitro transfection is coincident with extracellular release of PEG and increased uptake of the nanoparticle. The reducible PEGylation permits maintenance of the benefits of PEG, i.e., reduced aggregation, increased solubility, and in vivo transfection, while restoring transfection by the nanoparticles in vitro, thereby making in vitro study of intracellular trafficking of the relevant nanoparticle accessible. We consider the PEG-SS-POD/DNA nanoparticle to provide a valuable tool in development of this technology for gene therapy for ocular diseases.

MATERIALS AND METHODS

Reagents

POD peptide [CGGG(ARKKAAKA)$_4$] was synthesized and purified by high-performance liquid chromatography at Tufts University

Peptide Synthesis Core Facility (Tufts University). Methoxy-PEG-orthopyridyl disulfide (mPEG-OPSS; molecular weight [MW], 10,000) and mPEG-MALM (MW 10,000) were purchased from Laysan Bio. Ellman's reagent [5, 5′-dithio-bis-(2-nitrobenzoic acid); DTNB] was purchased from Sigma. Plasmid labeling kit was purchased from Mirus Bio. Cell culture reagents were purchased Life Technologies. Micro Bio-Spin P6 chromatography columns, Any kD TGX protein gels, and Quick Start Bradford Protein Assay were purchased from Bio-Rad. Luciferase Assay System was purchased from Promega. Barium chloride was purchased from Thermo Fisher Scientific. The LDH kit was purchased from ScienCell Research Laboratories.

Cloning

The plasmids pCAGLuc and pCAGLacZ were described previously.[18] The plasmid pCAGhFLT1 was constructed by Cyagen Biosciences. The hFLT1(s7) encoding cDNA from pUNO1-hFLT1(s7) (Invivogen) was cloned into pCAGEN.[45]

Conjugation of PEG with POD and Plasmid Compaction

PEGylation of POD peptide and DNA compaction was performed as previously described,[18] with some modifications. In brief, POD peptide, mPEG-MALM, and mPEG-OPSS were dissolved in 0.1 mM sodium phosphate buffer containing 5 mM EDTA. PEGylation of POD via a thioether linkage (i.e., PEG-S-POD) was made by mixing 1:1 molar ratio of POD:mPEG-MALM. PEGylation of POD via a disulfide linkage (i.e., PEG-SS-POD) was prepared using a 2:1 molar ratio of mPEG-OPSS:POD. The reaction mixture was incubated overnight at room temperature on a shaker. PEGylated POD was then purified using Micro Bio-Spin P6 chromatography columns equilibrated with either 50 mM AmAc or 0.1% TFA. The PEG-S-POD and PEG-SS-POD were quantified by SDS-PAGE analysis alongside POD standards of known concentration using Any kD Mini-PROTEAN TGX protein gels. DNA was compacted by adding dropwise to either PEG-S-POD or PEG-SS-POD in a final nitrogen: phosphate ratio of 8:1. The resulting PEG-S-POD/DNA and PEG-SS-POD/DNA nanoparticles, respectively, were dialyzed in 5% dextrose using BioMax 10K centrifugal filters (Millipore) and stored at 4°C. Plasmid compaction was verified by reduced mobility through a 1% agarose gel. Plasmid DNA was released from nanoparticle by 15 min incubation with 0.25% trypsin at 37°C. DLS analysis was performed using a 90 Plus zeta sizer (Brookhaven) to measure the hydrodynamic diameter of nanoparticles in a diluted sample placed in a 3 mL cuvette.

Quantitation of Sulfhydryl Groups

Sulfhydryl groups were quantified using Ellman's reagent according to the manufacturer's instructions (Sigma). In brief, a DTNB stock solution (50 mM sodium acetate/2 mM DTNB) and a 1 M Tris (pH 8) solution were prepared. 1 μL of POD samples was diluted with 99 μL of DTNB working reagent (1:2:16.8 of DTNB stock:Tris solution:H_2O), and absorbance was read at 412 nm on a microplate reader (Molecular Devices) following a 5 min incubation. The concentration of thiols in the solution was determined by comparison with a series of cysteine standards.

Labeling of Plasmid DNA

For analysis of uptake of nanoparticles by ARPE-19 cells (American Type Culture Collection), plasmid DNA was labeled with the fluorophore Cy5, using a labeling kit from Mirus Bio according to the manufacturer's instructions. The ratio of Cy5 to plasmid used was 1:1 (v/w). The reaction mixture was incubated in a 50°C water bath in the dark for 3 hr.

Cell Culture, In Vitro Transfection, Luciferase Assay, and DTNB Inhibition

ARPE-19 cells were grown in DMEM supplemented with 10% fetal bovine serum. Cells were seeded in 96-well plates at an initial density of 4×10^4 cells/well at 1 day prior to transfection. At the time of transfection, the medium in each well was replaced with 100 μL of fresh Opti-MEM containing nanoparticles (to deliver 200 ng plasmid/well). Following a 24 hr incubation with nanoparticles at 37°C, the cells were harvested for luciferase assay. Luciferase activity was assessed using a luciferase assay kit according to manufacturer's protocol and a GloMax 20/20 Luminometer over a 10 s integration (Promega). Luciferase assay was normalized to total protein concentration and expressed as relative luciferase units (RLUs) per milligram protein. Protein concentration was measured using a Quick Start Bradford Protein Assay. For DTNB inhibition experiments, the cells were incubated for 30 min with DTNB dissolved in serum-free media at the indicated concentrations. The DTNB-containing media were aspirated and replaced with fresh serum-free media containing nanoparticles in the presence of the indicated concentration of DTNB for a further 1 hr 45 min. After 24 hr incubation, luciferase assay was performed on cell lysates. Experiments were performed three times independently.

Detection of PEG in Cell Culture Media

ARPE-19 cells were incubated with PEG-S-POD and PEG-SS-POD nanoparticles as described above. Following incubation at 37°C for the indicated times, the media were harvested and centrifuged at 10,000 rpm for 2 min at 4°C. The centrifuged media were analyzed by SDS-PAGE. Following electrophoresis, the gel was soaked in 5% barium chloride solution for 15 min, rinsed with distilled water for 30 min, and stained with 0.1 N iodine solution for 15 min. The positive control for dePEGylation was generated by incubation of PEG-SS-POD nanoparticles with 4 mM cysteine for 15 min.

LDH Assay

ARPE-19 cells were incubated with nanoparticles as described above. Following a 24 hr incubation, media were collected and LDH activity was measured using a kit provided by ScienCell Research Laboratories according to the recommended protocol.

Subretinal Injection and Laser Photocoagulation of Mice

All experiments involving animals were in accordance with the Statement for the Use of Animals in Ophthalmic and Vision Research. All animal procedures were approved by the Institutional Animal Care and Use Committee (IACUC) of Tufts University. C57BL/6J mice between 6 and 8 weeks were purchased from Jackson Laboratories and

maintained in a 12 hr dark/12 hr light cycle in accordance with federal, state, and local regulations. Subretinal injections of nanoparticles containing 1 μg of plasmid DNA in a 2 μL volume were performed with a 32G needle (Becton Dickinson) and a 5 μL glass syringe (Hamilton) by a transscleral transchoroidal approach. Two days after injection, animals were sacrificed by CO_2 inhalation followed by cervical dislocation and eyes processed for luciferase assay. The eyes were harvested and the anterior chamber was removed. The posterior eyecup was homogenized using a VWR PowerMax AHS 200 homogenizer (VWR). Laser photocoagulation was performed as previously described.[46] In brief, mice were sedated with an intraperitoneal injection of ketamine (0.1 g/kg)/xylazine (0.01 g/kg), and pupils were dilated with 2.5% phenylephrine HCl (Bausch & Lomb) and 1% tropicamide (Bausch & Lomb). To minimize corneal injury, we applied 2.5% hypromellose (Goniovisc). Four laser spots were made per eye using an argon laser (532 nm, IRIS Medical Light Solutions, IRIDEM; IRIDEX) set to a spot size of 75 μm in diameter, 150 mW, and 100 ms pulse time.

Lectin Staining

One week following laser photocoagulation and nanoparticle injection, the animals were euthanized with CO_2, and the eyes were enucleated. The cornea and lens were removed and the eyecup fixed in 4% paraformaldehyde in 0.1 M phosphate buffer overnight at 4°C. The retina was then removed and the sclera/choroid/RPE complex washed in PBS, blocked in 5% BSA in PBS, and stained with 5 μg/μL fluorescein-conjugated isolectin (Vectashield) in PBS for 1 hr. Eyecups were flat mounted on glass slides and imaged using an inverted microscope (IX51; Olympus) with relevant filters, a digital camera (Retiga 2000R-FAST; Q-Imaging), and QCapture Pro software (Q-Imaging). CNV area pictures were imaged by fluorescence microscopy (Leica). CNV area was measured using ImageJ software (NIH).

LacZ Detection

PEG-SS-POD/DNA nanoparticles containing 1 μg of plasmid DNA were injected in the subretinal space of 6- to 8-week-old C57BL/6J mice, as described above. After 48 hr, eyes were enucleated, fixed in 0.25% glutaraldehyde for 30 min, and washed three times in PBS for 30 min. The eyes were incubated in X-Gal solution (FisherBiotech, Fisher Scientific) for 16–18 hr and then rinsed in phosphate buffer (pH 7.4) for 45 min. The eyes were fixed for 24 hr in 4% paraformaldehyde (PFA), dehydrated, embedded, and 14 μm sections collected. Bright-field images were taken using an Olympus BX51 upright microscope (Olympus) with Q-capture Pro software.

qRT-PCR

At 2 days after laser and injection of PEG-SS-POD/pCAGhFLT1 and PEG-SS-POD/pCAGLuc nanoparticles, eyes were harvested and the cornea, lens, iris, and optic nerve removed. The remaining tissue was homogenized in RLT buffer (QIAGEN) using a VWR AHS200 homogenizer. Total RNA was purified using an RNeasy kit (QIAGEN) according to the manufacturer's instructions. In brief, RNA was isolated on silica membrane columns using an on-column DNase treatment. qRT-PCR was performed using 100 ng of total RNA and 900 nM human sFLT1 primers (sFLT1 forward, 5′-CATA GATGTCCAAATAAGCAC-3′; sFLT1 reverse, 5′-CGAGTCAAA TAG CGAGCAGAT-3′) with iTaq Universal SYBR Green One-Step kit (Bio-Rad) in a 10 μL reaction. The reaction mix included an iScript Reverse Transcriptase and an antibody-mediated hot-start iTAQ DNA polymerase and was incubated at 50°C for 10 min followed by 1 min at 95°C and 40 cycles of 95°C for 10 s, 60°C for 30 s, and 72°C for 60 s on a multicolor real-time PCR detection system (iQ5; Bio-Rad) using optical system software. qRT-PCR of known amounts of pCAGhFLT1 plasmid was performed, and a standard curve of transgene copy number versus threshold cycle generated. The standard curve was used to calculate the number of copies of hFLT1 mRNA in the total RNA isolated from injected eyecups.

Western Blotting

ARPE-19 cells were transfected with pCAGhFLT1 and control plasmids as described above. After 24 hr, the media were harvested and concentrated using a 30K Amicon Ultra centrifugal filter. The media were loaded and electrophoresed on an Any kD gel as described above and transferred onto a membrane. After blocking with Odyssey blocking buffer (LI-COR Biosciences) for 1 hr, the membrane was incubated at room temperature for 1 hr with rabbit monoclonal [Y103] to VEGF receptor 1 (ab32152; Abcam). The membrane was subsequently incubated at room temperature for 1 hr with IRDye 800CW anti-(rabbit IgG) antibody and visualized using an Odyssey IR imaging system (LI-COR Biosciences).

Statistical Analysis

All data analyses were performed using Prism Software 5 (GraphPad Software). In experiments comparing three or more samples, data were analyzed using a one-way analysis of variance with a post hoc Tukey multiple comparison test for significance. All other statistical tests were performed using an unpaired Students t test. All data are presented as the mean ± SE.

AUTHOR CONTRIBUTIONS

Study Design: R.K.-S., B.C.D., and S.M.C.; Experiment Design and Implementation: B.C.D. and S.M.C.; Data Analysis: B.C.D. and S.M.C.; Manuscript Preparation: B.C.D. and S.M.C.; Manuscript Review and Editing: R.K.-S.; Funding Acquisition, R.K.-S.

ACKNOWLEDGMENTS

This study was supported by grants to R.K.-S. from the National Institutes of Health/NEI (EY021805 and EY013837), the Department of Defense/CDMRP (W81XWH-12-1-0374 and W81XWH-16-1-0650), The Ellison Foundation, and The Paul and Phyllis Fireman Foundation. We wish to thank Dr. Srinivas Sridhar and Dr. Rajiv Kumar (Northeastern University) for providing access to a Zetasizer for these studies.

REFERENCES

1. Bryant, L.M., Christopher, D.M., Giles, A.R., Hinderer, C., Rodriguez, J.L., Smith, J.B., Traxler, E.A., Tycko, J., Wojno, A.P., and Wilson, J.M. (2013). Lessons learned from

the clinical development and market authorization of Glybera. Hum. Gene Ther. Clin. Dev. *24*, 55–64.

2. Nathwani, A.C., Tuddenham, E.G., Rangarajan, S., Rosales, C., McIntosh, J., Linch, D.C., Chowdary, P., Riddell, A., Pie, A.J., Harrington, C., et al. (2011). Adenovirus-associated virus vector-mediated gene transfer in hemophilia B. N. Engl. J. Med. *365*, 2357–2365.
3. Hauswirth, W.W., Aleman, T.S., Kaushal, S., Cideciyan, A.V., Schwartz, S.B., Wang, L., Conlon, T.J., Boye, S.L., Flotte, T.R., Byrne, B.J., and Jacobson, S.G. (2008). Treatment of leber congenital amaurosis due to RPE65 mutations by ocular subretinal injection of adeno-associated virus gene vector: short-term results of a phase I trial. Hum. Gene Ther. *19*, 979–990.
4. Maguire, A.M., Simonelli, F., Pierce, E.A., Pugh, E.N., Jr., Mingozzi, F., Bennicelli, J., Banfi, S., Marshall, K.A., Testa, F., Surace, E.M., et al. (2008). Safety and efficacy of gene transfer for Leber's congenital amaurosis. N. Engl. J. Med. *358*, 2240–2248.
5. Bainbridge, J.W., Smith, A.J., Barker, S.S., Robbie, S., Henderson, R., Balaggan, K., Viswanathan, A., Holder, G.E., Stockman, A., Tyler, N., et al. (2008). Effect of gene therapy on visual function in Leber's congenital amaurosis. N. Engl. J. Med. *358*, 2231–2239.
6. Samulski, R.J., and Muzyczka, N. (2014). AAV-mediated gene therapy for research and therapeutic purposes. Annu Rev Virol *1*, 427–451.
7. Chamberlain, K., Riyad, J.M., and Weber, T. (2016). Expressing transgenes that exceed the packaging capacity of adeno-associated virus capsids. Hum. Gene Ther. Methods *27*, 1–12.
8. Mingozzi, F., and High, K.A. (2011). Immune responses to AAV in clinical trials. Curr. Gene Ther. *11*, 321–330.
9. Chandler, R.J., LaFave, M.C., Varshney, G.K., Trivedi, N.S., Carrillo-Carrasco, N., Senac, J.S., Wu, W., Hoffmann, V., Elkahloun, A.G., Burgess, S.M., and Venditti, C.P. (2015). Vector design influences hepatic genotoxicity after adeno-associated virus gene therapy. J. Clin. Invest. *125*, 870–880.
10. Wang, L., Blouin, V., Brument, N., Bello-Roufai, M., and Francois, A. (2011). Production and purification of recombinant adeno-associated vectors. Methods Mol. Biol. *807*, 361–404.
11. Mintzer, M.A., and Simanek, E.E. (2009). Nonviral vectors for gene delivery. Chem. Rev. *109*, 259–302.
12. Rettig, G.R., and Rice, K.G. (2007). Non-viral gene delivery: from the needle to the nucleus. Expert Opin. Biol. Ther. *7*, 799–808.
13. van Gaal, E.V., van Eijk, R., Oosting, R.S., Kok, R.J., Hennink, W.E., Crommelin, D.J., and Mastrobattista, E. (2011). How to screen non-viral gene delivery systems in vitro? J. Control. Release *154*, 218–232.
14. Vercauteren, D., Rejman, J., Martens, T.F., Demeester, J., De Smedt, S.C., and Braeckmans, K. (2012). On the cellular processing of non-viral nanomedicines for nucleic acid delivery: mechanisms and methods. J. Control. Release *161*, 566–581.
15. Ni, R., Zhou, J., Hossain, N., and Chau, Y. (2016). Virus-inspired nucleic acid delivery system: Linking virus and viral mimicry. Adv. Drug Deliv. Rev. *106* (Pt A), 3–26.
16. Schuster, B.S., Ensign, L.M., Allan, D.B., Suk, J.S., and Hanes, J. (2015). Particle tracking in drug and gene delivery research: state-of-the-art applications and methods. Adv. Drug Deliv. Rev. *91*, 70–91.
17. Johnson, L.N., Cashman, S.M., and Kumar-Singh, R. (2008). Cell-penetrating peptide for enhanced delivery of nucleic acids and drugs to ocular tissues including retina and cornea. Mol. Ther. *16*, 107–114.
18. Read, S.P., Cashman, S.M., and Kumar-Singh, R. (2010). A poly(ethylene) glycolylated peptide for ocular delivery compacts DNA into nanoparticles for gene delivery to post-mitotic tissues in vivo. J. Gene Med. *12*, 86–96.
19. Read, S.P., Cashman, S.M., and Kumar-Singh, R. (2010). POD nanoparticles expressing GDNF provide structural and functional rescue of light-induced retinal degeneration in an adult mouse. Mol. Ther. *18*, 1917–1926.
20. Hornig, C., Barleon, B., Ahmad, S., Vuorela, P., Ahmed, A., and Weich, H.A. (2000). Release and complex formation of soluble VEGFR-1 from endothelial cells and biological fluids. Lab. Invest. *80*, 443–454.
21. Farjo, R., Skaggs, J., Quiambao, A.B., Cooper, M.J., and Naash, M.I. (2006). Efficient non-viral ocular gene transfer with compacted DNA nanoparticles. PLoS ONE *1*, e38.
22. Visentini, J., Gauthier, J., and Bertrand, M.J. (1989). Effect of trifluoroacetic acid on the reduction of disulfide bridges in peptides analyzed by fast-atom bombardment mass spectrometry. Rapid Commun. Mass Spectrom. *3*, 390–395.
23. Patel, V.R., and Agrawal, Y.K. (2011). Nanosuspension: an approach to enhance solubility of drugs. J. Adv. Pharm. Technol. Res. *2*, 81–87.
24. Bauer, W.R., Crick, F.H., and White, J.H. (1980). Supercoiled DNA. Sci. Am. *243*, 100–113.
25. Chancham, P., and Hughes, J.A. (2001). Relationship between plasmid DNA topological forms and in vitro transfection. J. Liposome Res. *11*, 139–152.
26. Dhanoya, A., Chain, B.M., and Keshavarz-Moore, E. (2011). The impact of DNA topology on polyplex uptake and transfection efficiency in mammalian cells. J. Biotechnol. *155*, 377–386.
27. Breunig, M., Lungwitz, U., Liebl, R., and Goepferich, A. (2007). Breaking up the correlation between efficacy and toxicity for nonviral gene delivery. Proc. Natl. Acad. Sci. USA *104*, 14454–14459.
28. Suk, J.S., Xu, Q., Kim, N., Hanes, J., and Ensign, L.M. (2016). PEGylation as a strategy for improving nanoparticle-based drug and gene delivery. Adv. Drug Deliv. Rev. *99* (Pt A), 28–51.
29. Romberg, B., Hennink, W.E., and Storm, G. (2008). Sheddable coatings for long-circulating nanoparticles. Pharm. Res. *25*, 55–71.
30. Sun, W., and Davis, P.B. (2010). Reducible DNA nanoparticles enhance in vitro gene transfer via an extracellular mechanism. J. Control. Release *146*, 118–127.
31. Alley, S.C., Benjamin, D.R., Jeffrey, S.C., Okeley, N.M., Meyer, D.L., Sanderson, R.J., and Senter, P.D. (2008). Contribution of linker stability to the activities of anticancer immunoconjugates. Bioconjug. Chem. *19*, 759–765.
32. Binder, C., Cashman, S.M., and Kumar-Singh, R. (2013). Extended duration of transgene expression from pegylated POD nanoparticles enables attenuation of photoreceptor degeneration. PLoS ONE *8*, e82295.
33. Strauss, O. (2005). The retinal pigment epithelium in visual function. Physiol. Rev. *85*, 845–881.
34. Yang, S., Li, H., Li, M., and Wang, F. (2015). Mechanisms of epithelial-mesenchymal transition in proliferative vitreoretinopathy. Discov. Med. *20*, 207–217.
35. Han, J.W., Lyu, J., Park, Y.J., Jang, S.Y., and Park, T.K. (2015). Wnt/β-catenin signaling mediates regeneration of retinal pigment epithelium after laser photocoagulation in mouse eye. Invest. Ophthalmol. Vis. Sci. *56*, 8314–8324.
36. Lee, S.H., Kim, H.D., Park, Y.J., Ohn, Y.H., and Park, T.K. (2015). Time-dependent changes of cell proliferation after laser photocoagulation in mouse chorioretinal tissue. Invest. Ophthalmol. Vis. Sci. *56*, 2696–2708.
37. Kwak, N., Okamoto, N., Wood, J.M., and Campochiaro, P.A. (2000). VEGF is major stimulator in model of choroidal neovascularization. Invest. Ophthalmol. Vis. Sci. *41*, 3158–3164.
38. Aguilar, E., Dorrell, M.I., Friedlander, D., Jacobson, R.A., Johnson, A., Marchetti, V., Moreno, S.K., Ritter, M.R., and Friedlander, M. (2008). Chapter 6. Ocular models of angiogenesis. Methods Enzymol. *444*, 115–158.
39. Watson, W.H., Ritzenthaler, J.D., and Roman, J. (2016). Lung extracellular matrix and redox regulation. Redox Biol. *8*, 305–315.
40. Ishida, T., Kirchmeier, M.J., Moase, E.H., Zalipsky, S., and Allen, T.M. (2001). Targeted delivery and triggered release of liposomal doxorubicin enhances cytotoxicity against human B lymphoma cells. Biochim. Biophys. Acta *1515*, 144–158.
41. Lei, Y., Wang, J., Xie, C., Wagner, E., Lu, W., Li, Y., Wei, X., Dong, J., and Liu, M. (2013). Glutathione-sensitive RGD-poly(ethylene glycol)-SS-polyethylenimine for intracranial glioblastoma targeted gene delivery. J. Gene Med. *15*, 291–305.
42. Igarashi, T., Miyake, K., Masuda, I., Takahashi, H., and Shimada, T. (2010). Adeno-associated vector (type 8)-mediated expression of soluble Flt-1 efficiently inhibits neovascularization in a murine choroidal neovascularization model. Hum. Gene Ther. *21*, 631–637.

43. Ahmed, A., Dunk, C., Ahmad, S., and Khaliq, A. (2000). Regulation of placental vascular endothelial growth factor (VEGF) and placenta growth factor (PIGF) and soluble Flt-1 by oxygen—a review. Placenta *21* (*Suppl. A*), S16–S24.

44. Lai, C.M., Shen, W.Y., Brankov, M., Lai, Y.K., Barnett, N.L., Lee, S.Y., Yeo, I.Y., Mathur, R., Ho, J.E., Pineda, P., et al. (2005). Long-term evaluation of AAV-mediated sFlt-1 gene therapy for ocular neovascularization in mice and monkeys. Mol. Ther. *12*, 659–668.

45. Matsuda, T., and Cepko, C.L. (2004). Electroporation and RNA interference in the rodent retina in vivo and in vitro. Proc. Natl. Acad. Sci. USA *101*, 16–22.

46. Cashman, S.M., Ramo, K., and Kumar-Singh, R. (2011). A non membrane-targeted human soluble CD59 attenuates choroidal neovascularization in a model of age related macular degeneration. PLoS ONE *6*, e19078.